

# PaMi-VDPO: Mitigating Video Hallucinations by Prompt-Aware Multi-Instance Video Preference Learning

Xinpeng Ding<sup>1</sup>, Kui Zhang<sup>2</sup>, Jianhua Han<sup>2</sup>, Lanqing Hong<sup>2</sup>, Hang Xu<sup>2</sup>, Xiaomeng Li<sup>1</sup>

<sup>1</sup>The Hong Kong University of Science and Technology

<sup>2</sup>Huawei Noah’s Ark Lab

## Abstract

*Direct Preference Optimization (DPO) helps reduce hallucinations in Video Multimodal Large Language Models (VLLMs), but its reliance on offline preference data limits adaptability and fails to capture true video-response misalignment. We propose Video Direct Preference Optimization (VDPO), an online preference learning framework that eliminates the need for preference annotation by leveraging video augmentations to generate rejected samples while keeping responses fixed. However, selecting effective augmentations is non-trivial, as some clips may be semantically identical to the original under specific prompts, leading to false rejections and disrupting alignment. To address this, we introduce **Prompt-aware Multi-instance Learning VDPO (PaMi-VDPO)**, which selects augmentations based on prompt context. Instead of a single rejection, we construct a candidate set of augmented clips and apply a close-to-far selection strategy, initially ensuring all clips are semantically relevant while then prioritizing the most prompt-aware distinct clip. This allows the model to better capture meaningful visual differences, mitigating hallucinations, while avoiding false rejections, and improving alignment. PaMi-VDPO seamlessly integrates into existing VLLMs without additional parameters, GPT-4/human supervision. With only 10k SFT data, it improves the base model by 5.3% on Video-Hallucer, surpassing GPT-4o, while maintaining stable performance on general video benchmarks.*

## 1. Introduction

Video multi-modal large language models (VLLMs) [14, 15, 23, 24, 52] have demonstrated remarkable capabilities in video understanding tasks, such as video question answering and captioning [6, 7, 16, 20, 28, 46]. However, these models suffer from a persistent challenge: hallucination [25], where generated responses deviate from actual visual content. While hallucination in image-based MLLMs has been widely studied [9–11, 18, 36, 39–42, 48, 49], its impact and

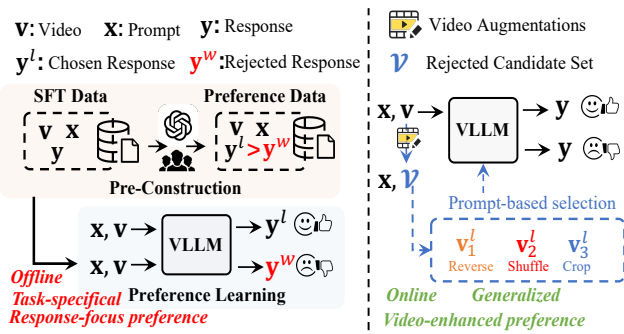


Figure 1. **Comparison of different methods.** **Left:** Direct Preference Optimization (DPO) requires costly LLMs or human annotators to preconstruct preference data offline for different tasks, limiting its generalization. Meanwhile, its preference learning only applies to responses, ignoring the involvement of the video. **Right:** Our Prompt-aware Multi-instance learning Video DPO (PaMi-VDPO) overcomes these limitations by *constructing a candidate rejected video set during training and automatically selects the appropriate rejected video based on the prompt to perform video-enhanced preference learning*.

mitigation in VLLMs remain largely unexplored.

Existing efforts to mitigate hallucination in VLLMs fall into two main categories. **(i) Architectural modifications**, such as VISTA-LLAMA [27], which alter attention mechanisms to reduce hallucinations. However, these modifications require retraining for different tasks and hinder the use of efficient implementations like FlashAttention [5]. **(ii) Preference learning**, particularly Direct Preference Optimization (DPO) [45], which trains models to prefer more reliable responses over hallucinated ones based on the constructed video preference data.

While effective, DPO has several limitations, as shown in Fig. 1(a): **(i) High cost of pre-construction.** DPO relies on human annotators or powerful LLMs to generate high-quality preference data, making it costly and labor-intensive. **(ii) Offline limitation.** Preference data is generated before training, leading to two major drawbacks: **lack of adaptability**, as offline data cannot adjust to new tasks or scenarios, and **data staleness**, where pre-constructed data may become outdated

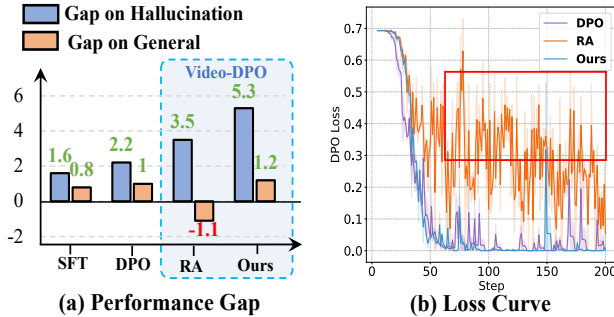


Figure 2. **Impact of Augmentations.** RA: Random video augmentation. (a) **Performance gap** with the base model (LLaVA-OV-7B [13]) and (b) **DPO loss curve** show that RA leads to performance degradation on general benchmarks and unstable training (red box). Performance gains and degradation are highlighted in green and red, respectively. In contrast, our Prompt-aware Multi-instance learning Video DPO (PaMi-VDPO) achieves superior performance on both hallucination and general benchmarks while ensuring stable training.

and misaligned with evolving models and task requirements. **(iii) Response-focused preference.** Since optimization primarily targets response alignment, the model may prioritize linguistic style over addressing misalignment with visual content [36] (see in Fig. 7).

To address these limitations, this paper introduces a novel attempt, **Video DPO (VDPO)**, a video-centric online preference learning that obviates the requirement for pre-constructed preference data. Rather than annotating text responses, VDPO applies *video augmentations to generate rejected video clips while sharing the original response*. By training the model to prefer the original video over its augmented variants, VDPO explicitly enforces video-response alignment, mitigating hallucinations based on visual content rather than textual style. Unlike traditional DPO, VDPO is entirely self-supervised, making it more scalable and adaptable to various video tasks.

Through our experiments in Section 4.2, we identify *augmentation selection as a crucial bottleneck in VDPO*, significantly impacting its effectiveness. A fundamental challenge lies in the trade-off between **general semantic similarity** and **prompt<sup>1</sup>-based distinctiveness**. On one hand, the augmented rejected clips should maintain high semantic similarity with the original to help the model detect subtle inconsistencies for mitigating hallucinations (Fig. 3(b)). On the other hand, overly similar rejected clips can lead to false-rejected samples, *i.e.*, where the rejected clips are semantically identical to the original clip under specific prompts (Fig. 4). This false-rejected issue would introduce alignment noise, leading to unstable training and suboptimal performance, as shown in Fig. 2 (RA).

To address this, we propose **Prompt-aware Multi-instance Learning VDPO (PaMi-VDPO)**, a novel framework that au-

tomatically constructs multiple candidates, allowing our model to dynamically adjust its preference learning based on prompts while mitigating interference from false-rejected noise. PaMi-VDPO is performed in a **close-to-far strategy**: We first generate a candidate set of rejected clips using high-similarity augmentations, ensuring that rejected samples remain visually close to the original video while capturing subtle hallucinations. Then, we select the most divergent augmented clip—*i.e.*, the one whose response deviates most from the original—as the pseudo true-rejected sample. By dynamically prioritizing the most misaligned sample while down-weighting others, PaMi-VDPO seamlessly integrates prompt-dependent augmentation selection into preference learning through a multi-instance learning (MIL) approach. Notably, PaMi-VDPO requires no additional parameters, no architectural modifications, and no manually curated preference data, making it efficient and easily integrated into existing VLLM training pipelines.

**Contributions.** Our main contributions are:

- We introduce Video DPO (VDPO), the first video-centric online preference learning framework that directly enforces video-response alignment through video augmentations, eliminating the reliance on pre-constructed preference data.
- We identify false rejection in video augmentations as a critical bottleneck in VDPO, where rejected clips remain overly semantic-similar to the original under the given prompt, introducing alignment noise.
- We propose PaMi-VDPO, allowing the model to leverage the prompt information to adaptively learn from diverse augmented clips while suppressing noise ones to avoid false-rejected issues, improving stability and effectiveness.
- Our approach achieves state-of-the-art hallucination mitigation while ensuring stable general performance, without requiring additional preference data, model parameters, or architectural modifications.

## 2. Related Work

### 2.1. Hallucination in image and video MLLMs

**Image Hallucination.** Multimodal large language models (MLLMs) often generate responses misaligned with visual content [25]. Existing mitigation methods fall into two categories: (i) Post-processing, which refines model outputs after generation [10, 11, 40, 48, 49], but adds inference overhead. (ii) Data-driven preference alignment, where methods like Hallucidocor [41] and LRV-Instruction [22] improve dataset quality, while DPO-based approaches [18, 33, 36, 42] enhance alignment with visual content.

**Video Hallucination.** Most video hallucination mitigation methods extend image-based strategies. VISTALLAMA [27] modifies attention mechanisms, improving alignment but limiting scalability for long videos. LLAVALHOUND-DPO [45] applies DPO with GPT-4V-generated

<sup>1</sup>“Prompt” is also referred to as “question” or “instruction.”

preference data, but relies on expensive, closed-source APIs [30]. However, its reliance on offline preference data limits adaptability, would be outdated as the model evolves, and overlooks true video-response misalignment.

Unlike existing approaches, our method mitigates video hallucinations without modifying the architecture or relying on costly preference data generation, and conducts preference learning in an online manner.

## 2.2. Direct preference optimization in MLLMs

Preference optimization [34], particularly Direct Preference Optimization (DPO) [29, 33], has been widely used to align multimodal LLMs (MLLMs) with visual content [18, 31, 32, 36, 36, 39, 42, 53]. DPO relies on high-quality preference data, typically consisting of an image, a prompt, and two responses: one preferred (aligned with the image) and one rejected (more hallucinated). These annotations are often generated using multiple model responses [18] or augmented from different seeds [42, 45], with labels from GPT-4o [30] or human. To further improve alignment, some works [9, 39, 53] modify the standard DPO objective by keeping responses fixed while perturbing the image to generate visually misaligned samples. This method has shown effectiveness in mitigating hallucinations in image-based MLLMs, as it enforces models to distinguish subtle visual differences.

Due to the additional temporal dimension, selecting augmentations for video DPO is non-trivial, generally suffers from false-rejected issues (see more in Section 4). To this end we introduce PaMi-VDPO, a novel prompt multi-instance learning framework, significantly reducing false rejections while maintaining computational efficiency.

## 3. Preliminary

In this section, we briefly review how existing approaches leverage direct preference optimization (DPO) to improve the performance of multimodal large language models (MLLMs), especially for mitigating hallucinations.

**Supervised Fine-tuning (SFT).** In this stage, we have the training SFT data  $\mathcal{D}_{\text{SFT}} = \{(\mathbf{x}, \mathbf{v}, \mathbf{y})\}$  where  $x$ ,  $v$  and  $y$  are the instruction prompt, visual input and response respectively. Then, the MLLM with parameters  $\pi_\theta$  is trained to maximize the log-likelihood of  $y$  given  $x$  and  $v$  with the cross-entropy loss in the autoregressive manner [23]. We follow the previous works [18, 42] that regard the model after the SFT stage as the reference model  $\pi_{\text{ref}}$ .

**Direct Preference Optimization (DPO).** Recent approaches leverage DPO to further enhance the response quality of MLLMs and reduce hallucinations. Specifically, the pair-wise preference data is formulated as  $\mathcal{D}_{\text{DPO}} = \{(\mathbf{x}, \mathbf{v}, \mathbf{y}^w, \mathbf{y}^l)\}$ , where  $\mathbf{y}^w$  is the chosen response which is preferred the rejected response  $\mathbf{y}^l$ . Based on the constructed

preference data, the DPO loss [42] can be formulated as:

$$\mathcal{L}_{\text{dpo}} = -\log \sigma [\beta * (\mathcal{R}(\mathbf{y}^w | \mathbf{x}, \mathbf{v}) - \mathcal{R}(\mathbf{y}^l | \mathbf{x}, \mathbf{v}))], \quad (1)$$

where  $\beta$  controls the deviation  $\pi_\theta$  from  $\pi_{\text{ref}}$  during the optimization.  $\mathcal{R}(\mathbf{y}^w | \mathbf{x}, \mathbf{v})$  and  $\mathcal{R}(\mathbf{y}^l | \mathbf{x}, \mathbf{v})$  are the chosen and rejected rewards, defined as follows:

$$\mathcal{R}(\mathbf{y}^w | \mathbf{x}, \mathbf{v}) = \log \left( \frac{\pi_\theta(\mathbf{y}^w | \mathbf{x}, \mathbf{v})}{\pi_{\text{ref}}(\mathbf{y}^w | \mathbf{x}, \mathbf{v})} \right), \quad (2)$$

where  $\pi_{\text{ref}}$  is the fixed reference model,  $\pi_\theta$  is the trained model during the DPO.

## 4. Video Preference Learning

### 4.1. Overall Framework

Direct Preference Optimization (DPO) has been applied to mitigate hallucinations in VLLMs by preconstructing preference data (correct vs. hallucinated responses). However, it suffers from high annotation costs, offline data limitations, and response-focused learning biases. To overcome these issues, we introduce **Video DPO (VDPO)**, which removes the need for manually curated preference data by enforcing preference learning directly on videos.

As shown in Fig. 3 (a), VDPO consists of three steps: (i) Sampling training examples  $\{\mathbf{x}, \mathbf{y}, \mathbf{v}^w\}$  from SFT datasets; (ii) Applying video augmentations to the original video clip  $\mathbf{v}^w$  to generate the rejected video clip  $\mathbf{v}^l$ ; (iii) Optimizing the model (e.g., LLaVA-OV-7B [13]) using the VDPO objective:

$$\mathcal{L}_{\text{vdpo}} = -\log \sigma [\beta * (\mathcal{R}(\mathbf{y} | \mathbf{x}, \mathbf{v}^w) - \mathcal{R}(\mathbf{y} | \mathbf{x}, \mathbf{v}^l))]. \quad (3)$$

### 4.2. Augmentation: A Bottleneck in VDPO

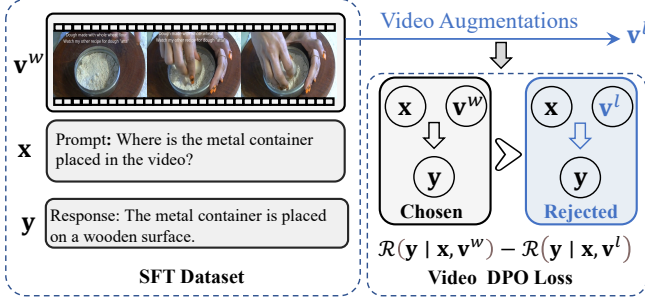
As Eq. 3 shows, the only variable in VDPO is the video input, meaning that the construction of the rejected clip plays a crucial role in its effectiveness. A key question arises: *What kinds of video augmentations are optimal for VDPO?*

To answer this, we conduct an empirical study analyzing the impact of different augmentations.

#### 4.2.1. Experiment Setup

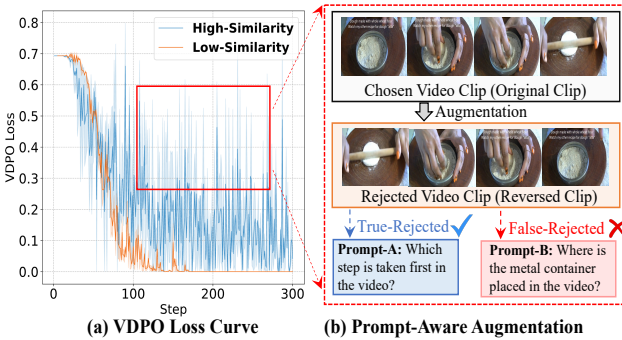
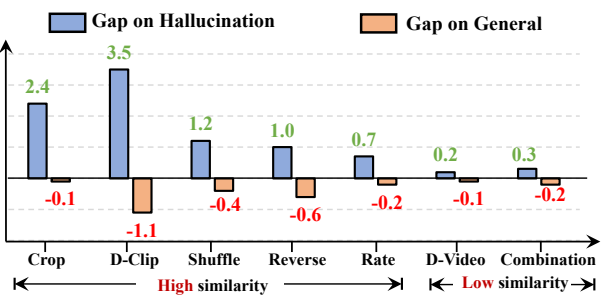
**Training Data.** We sample 10K SFT examples from *Temporal-Bench* [3] and *LLaVA-Video-178k* [47] to evaluate performance across temporal and visual domains.

**Augmentation Strategies.** We apply the following video augmentations to construct rejected clips: (1) **Crop** – randomly cropping less than 20% of the frame from the original video; (2) **D-video** – randomly selecting clips from another video from the training data; (3) **D-Clip** – selecting another clip from the same long video with the original video clip. (4) **Shuffle** – shuffling the temporal order of the original video clip; (5) **Reverse** – reversing the original temporal order; (6) **Rate** – sampling frames from the original video



(a) Video DPO Pipeline

Figure 3. (a) **Video DPO (VDPO) Pipeline.** VDPO applies augmentations to the original clip  $v^w$  to generate the rejected clip  $v^l$ , then optimized by the VDPO objective (Eq. 3). (b) **Performance Gap Across Different Augmentations.** The x-axis represents different augmentation strategies for generating rejected clips, while the y-axis shows the performance gap relative to the baseline (LLaVA-OV-7B [13]) across hallucination and general benchmarks (see Section 4.2.1). Gains and degradations are highlighted in green and -red, respectively. **High-similarity** augmentations retain semantic closeness to the original clip, whereas **low-similarity** ones introduce significant differences (see more in Section 4.2.1). Different augmentation strategies have a substantial impact on VDPO performance, analyzed further in Section 4.2.2.



(a) VDPO Loss Curve

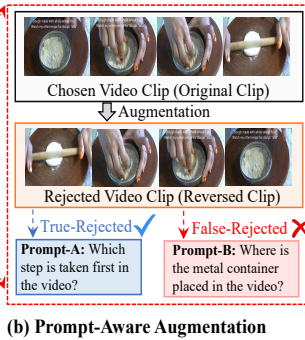


Figure 4. (a) **VDPO loss curve.** The solid line depicts the average loss, with the shaded area showing the variance. *VDPO* loss trained with high-similarity augmentations exhibits greater variance, whereas low-similarity augmentations enable smoother convergence. (b) **Prompt-aware augmentation.** The impact of augmentations varies by prompts, i.e., the augmented rejected video clip may have the same response as the chosen clip for some prompts. We term these generated clips as false-rejected.

clip at a different frame rate; (7) **Combination** – applying two ways sampled from previous augmentation strategies.

For further analysis, we categorize the above augmentations into two groups: (i) **High-similarity Augmentations**: augmentations that do not significantly alter the semantic content of the original video clip, resulting in a high similarity between the augmented and original clips. (ii) **Low-similarity Augmentations**: augmentations that significantly alter the original semantic content, making it difficult or impossible to recognize the original scene or objects.

**Evaluation Metrics.** We evaluate models on: - General Benchmarks: Average performance on *TempCompass* [26], *NextQA* [38] and *Video-MME* [26]. - Hallucination Benchmarks: Five sub-tasks from *VideoHallucer* [37].

#### 4.2.2. Experimental Findings

##### High-Similarity Augmentations Improve Hallucination Mitigation.

As shown in Fig. 3 (b), VDPO models trained

with high-similarity augmentations outperform those using low-similarity augmentations. This is because high-similarity augmentations generate subtle yet distinguishable negative samples, forcing the model to focus on fine-grained video-response misalignment. For example, D-Clip achieves a +3.5% improvement in hallucination benchmarks.

**Low-Similarity Augmentations Provide Minimal Benefit.** Low-similarity augmentations create rejected clips with obvious semantic gaps, making it trivial for the model to distinguish between the original and rejected samples. As a result, these augmentations fail to provide meaningful supervision. Fig. 4 (a) shows that VDPO loss converges too quickly (orange curve), indicating ineffective learning.

**Instability of High-Similarity Augmentations.** Despite their benefits, high-similarity augmentations introduce training instability:

- **Performance sensitivity** – Gains vary widely by augmentation (e.g., D-Clip: +3.5%, Reverse: +1.0%).
- **General benchmark degradation** – High-similarity augmentations often cause a performance drop on general tasks (e.g., D-Clip: -1.1%).
- **Slow and unstable loss convergence** – As shown in Fig. 4 (a), high-similarity augmentations (blue curve) exhibit large variance and slower convergence.

**False-Rejected Issue in VDPO.** The effectiveness of an augmentation varies depending on the prompt. As shown in Fig. 4 (b), applying Reverse to generate a rejected clip is effective for Prompt-A (where event order matters) but fails for Prompt-B (where object positions remain unchanged). Such false-rejected samples disrupt VLLM alignment, leading to instability.

To validate this, we design a controlled experiment by curating temporal-related questions from the original SFT dataset. Specifically, we leverage the GPT-4o API [30] to identify questions involving temporal reasoning (e.g., direction prediction, velocity estimation, or sequential under-

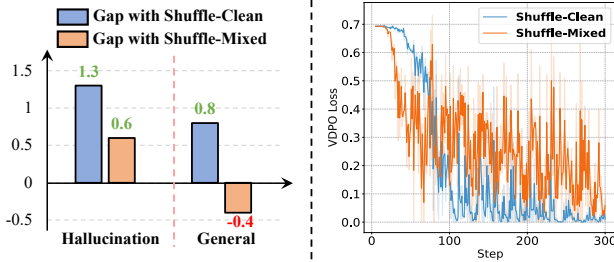


Figure 5. **Prompt-aware augmentation stabilizes VDPO.** Comparative analysis on both the performance gap (Left) and the loss curve (Right) reveals *selecting appropriate augmentations based on the questions can help mitigate VDPO instability*. Specifically, **Shuffle-Clean** and **Shuffle-Mixed** represent VDPO training with the Shuffle augmentation on Clean and Mixed data, respectively (see Section 4.2.2 for details). **Shuffle-Clean** consistently reduces hallucination and maintains generalizability, whereas **Shuffle-Mixed** degrades both the general tasks and optimization stability.

standing), resulting in 3K samples termed Clean data. For fair comparison, we randomly select 3K samples from the original dataset as Mixed data. Subsequently, we apply Shuffle augmentation to train two VDPO models: one on the Clean data (resulting in the Shuffle-Clean model) and the other on the Mixed data (resulting in the Shuffle-Mixed model). In Fig. 5, we report the performance gap of these models compared to a baseline model on hallucination and general benchmarks, as well as examining the training loss. Our results demonstrate that Shuffle-Clean significantly mitigates the instability of VDPO. This improvement stems from the fact that, for temporal-related questions in the Clean data, shuffled video clips are likely true-rejected, as shuffling disrupts the temporal information essential for accurate responses. Hence, tailoring augmentation strategies to the questions to avoid false-rejected is critical for addressing instability in VDPO training.

## 5. PaMi-VDPO

**The VDPO dilemma: hallucination vs. stability.** While VDPO mitigates hallucinations by enforcing preference learning on video inputs, it faces a fundamental trade-off in constructing rejected clips. On one hand, rejected clips should maintain high semantic similarity with the original to help the model detect subtle inconsistencies (Fig. 3(b)). On the other hand, overly similar rejected clips can lead to false-rejected samples, introducing alignment noise and destabilizing training (Fig. 4).

Our experiments in Fig. 5 suggest that prompt-dependent high-similarity augmentations can reduce false-rejected samples, but manually selecting these augmentations via human curation or LLM-based filtering is costly.

**Prompt-aware Multi-instance learning formulation.** To address this dilemma without relying on human/LLM pre-selection, we propose constructing a candidate set  $\mathcal{V}$  =

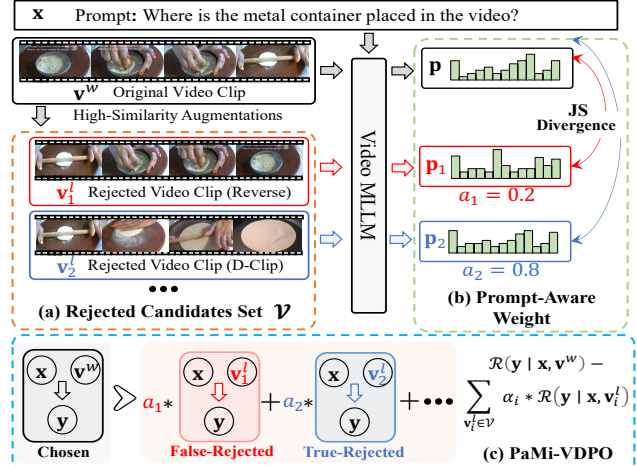


Figure 6. **Framework of our method.** Our method addresses VDPO’s instability caused by false-rejected clips through three key innovations: **(a) Rejected candidate set construction**  $\mathcal{V}$  that guarantees at least one is the true-rejected clip via multiple video augmentations; **(b) Prompt-Aware Weighting** that computes the Jensen-Shannon divergence between the LLM outputs of the original clip and those in  $\mathcal{V}$ , enabling us to identify the high-confidence rejected clip during training, without adding extra parameters; **(c) PaMi-VDPO Objective** emphasizes the high-confidence rejected candidates (blue boxes) while suppressing other samples (red boxes) during the preference learning.

$\{\mathbf{v}_i^l\}_{i=1}^N$  of  $N$  augmented video clips for each video-prompt pair  $\{\mathbf{x}, \mathbf{v}^w\}$ . Instead of relying on a single rejected clip, multiple candidates substantially increase the chance that **at least one true-rejected video clip** in  $\mathcal{V}$  aligns with the given prompt. As shown in Fig. 6 (a), among all the augmented clips  $\mathcal{V}$ , the one augmented by D-Clip  $\mathbf{v}_2^l$  is indeed the true-rejected clip matched with the prompt  $\mathbf{x}$ .

Notably, this candidate set aligns structurally with Multiple Instance Learning (MIL) [50], where  $\mathcal{V}$  serves as a bag containing both positive (true-rejected) and negative (false-rejected) instances. Consequently, we reformulate the VDPO objective (Eq. 3) into a Prompt-aware MIL VDPO (PaMi-VDPO) as follows:

$$\mathcal{L}_{\text{pami-vdpo}} = -\log \sigma \left[ \beta * \left( \mathcal{R}(\mathbf{y} | \mathbf{x}, \mathbf{v}^w) - \sum_{\mathbf{v}_i^l \in \mathcal{V}} \alpha_i * \mathcal{R}(\mathbf{y} | \mathbf{x}, \mathbf{v}_i^l) \right) \right], \quad (4)$$

where  $\alpha_i \in [0, 1]$  is a prompt-aware confidence score for clip  $\mathbf{v}_i^l$ . A higher  $\alpha_i$  suggests a stronger likelihood that  $\mathbf{v}_i^l$  is a pseudo true-rejected clip, while a lower  $\alpha_i$  implies potential noise (false-rejected). This MIL-based weighting scheme selectively optimizes high-confidence clips and suppresses noisy ones.

**Tailored designs for effectiveness.** To ensure that our MIL formulation effectively selects useful rejected samples, we introduce a **close-to-far** strategy, which balances the trade-

Models	VideoHallucer			EventHallusion		
	Basic	Hallu	Overall	Binary	Desc	Avg
VideoChatGPT [28]	92.8	10.4	6.4	47.19	11.6	29.4
VideoChat2 [17]	29.7	25.8	7.8	37.90	7.8	22.9
LLaMA-VID [19]	89.9	26.6	21.0	66.01	18.6	42.3
Video-LLaVA [20]	95.1	20.3	17.8	50.61	16.9	33.8
LLaVA-OV [13]	84.1	60.8	48.5	61.3	33.2	47.3
+ SFT	<b>85.1</b>	61.1	50.1 <small>(+1.6)</small>	66.0	30.7	48.4 <small>(+1.1)</small>
+ DPO	81.9	66.2	51.2 <small>(+2.7)</small>	<b>69.9</b>	31.7	50.8 <small>(+3.5)</small>
+ VDPO	75.5	67.9	51.1 <small>(+2.6)</small>	67.2	32.7	50.0 <small>(+2.7)</small>
+ PaMi-VDPO(ours)	82.8	<b>69.9</b>	<b>53.8</b> <small>(+5.3)</small>	<u>67.9</u>	<b>38.5</b>	<b>53.2</b> <small>(+5.9)</small>
<i>Proprietary models</i>						
Gemini-1.5-Pro [35]	83.6	42.3	37.8	80.2	49.6	64.9
GPT-4o [30]	75.1	74.2	53.5	84.1	56.2	70.2

Table 1. **Comparison with the stat-of-the-art MLLMs on hallucination benchmarks.** The LLM size of all models is around 7B. For all results, the higher value indicates a better performance. ‘AVG’ is the average performance. The best and the second-best values are marked in **Bold** and Underline. The performance gains is highlighted in (+blue). *Trained with the same data, our PaMi-VDPO outperforms SFT, DPO and VDPO across different backbones and benchmarks.*

off between retaining semantic similarity and avoiding false-rejected clips.

*Close construction:* We use diverse high-similarity augmentations to generate the rejected set  $\mathcal{V}$ . Because all clips in  $\mathcal{V}$  remain semantically close to the original, they help mitigate hallucinations (refer to Section 4.2.2 and Fig. 3(b)); meanwhile, diversity among these clips increases the likelihood of discovering true-rejected instances.

*Far selection:* We select the augmented clip that differs the most from the original clip’s LLM output as the true-rejected clip. Since LLM outputs depend on both the prompt and the video clip, a large output divergence indicates that the augmentation meaningfully affects the response. By emphasizing the farthest clip and down-weighting others, we reduce the risk of false-rejected noise.

Specifically, we measure the distance between outputs using the Jensen-Shannon (JS) divergence. Let  $\mathbf{p}^w$  be the MLLMs’ output logits for input  $\{\mathbf{x}, \mathbf{v}^w\}$  and  $\mathbf{p}_i^l$  be the logits for  $\{\mathbf{x}, \mathbf{v}_i^l\}$ . After converting logits to probabilities via softmax, we compute:

$$d_i = \text{JS}(\text{softmax}(\mathbf{p}^w) \parallel \text{softmax}(\mathbf{p}_i^l)). \quad (5)$$

We then derive prompt-aware confidence weights through a softmax over  $d_i$  values:

$$a_i = \frac{\exp(d_i)}{\sum_{j=1}^N \exp(d_j)}, \quad (6)$$

Notably, our framework introduces zero additional parameters and requires no architectural changes, making it straightforward to integrate into existing LLM training pipelines in a plug-and-play fashion.

Models	NextQA (mc)	VideoMME (wo sub.)	Tempcom (mc)	AVG
InternVL2-8B [4]	65.3	54.0	-	-
VILA-40B [21]	67.9	60.1	-	-
LongVA-7B [44]	68.3	52.6	-	-
LLaVA-OV [13]	79.4	58.2	64.8	67.5
LLaVA-OV*	77.8	58.4	64.8	67.0
+SFT	78.8	58.9	66.2	68.0 <small>(+1.0)</small>
+DPO	79.2	58.8	64.7	67.6 <small>(+0.6)</small>
+VDPO	77.8	56.7	63.3	65.9 <small>(-1.1)</small>
+PaMi-VDPO (ours)	79.7	58.5	66.4	68.2 <small>(+1.2)</small>

Table 2. **Comparison with the stat-of-the-art MLLMs on general benchmarks.** For all results, the higher value indicates a better performance. “\*” indicates the results reproduced by ourselves. The performance degradation is highlighted in (-red). *Compared with the standard DPO or VDPO, our PaMi-VDPO would not degrade the performance of general benchmarks, due to reducing the false-rejected clips.*

## 6. Experiments

### 6.1. Experimental settings

**Implementation Details.** We use LLaVA-OV-7B [13] as the backbone and train for 3 epochs with a learning rate of  $5e-7$  and batch size of 1. The number of sampled frames is 8 during training and 32 for inference. To improve efficiency, we apply  $2 \times 2$  average-pooling to the visual features of each frame. The candidate set size is fixed at 2 for an optimal balance between efficiency and performance. We use D-Clip (or Crop if D-Clip is unavailable) and Shuffle augmentations to construct the set. For further analysis, refer to Section 6.3 and **supplementary materials**.

**Training Data.** We sample around 10K SFT data examples from Temporal-bench [3] and LLaVA-Video-178k [47], the same as Section 4.2.1.

**Evaluation Benchmarks.** We evaluate our method on two hallucination (VideoHallucer [37], EventHallusion [43]) and three general (NextQA [38], Tempcompass (Tempcom) [26] and Video-MME (VMME) [8]) benchmarks. For hallucination benchmarks, we use their official evaluation code, while LMMS-Eval [12] for evaluating general benchmarks.

### 6.2. Comparison with state-of-the-art methods

We apply our method to a powerful VLLM, *i.e.*, LLaVA-OV [13]. For fair comparison, we also train the backbone using the same data by the supervised fine-tuning (SFT) and the standard DPO. The standard DPO requires the chosen and rejected response pairs for each data sample. To this end, for each sample, we first generate multiple responses by inputting different augmented videos, which are then annotated by a powerful model, *i.e.*, GPT-4o [30]. Refer to the **supplementary material** for more details. *Note, due to the lack of publicly available results where all models are evaluated on both hallucination and general benchmarks, we report them separately while ensuring our baseline (LLaVA-*

group	<i>Halluc</i>	<i>General</i>	type	<i>Halluc</i>	<i>General</i>	$\alpha_i$ in Eq. 6	<i>Halluc</i>	<i>General</i>	$d_i$ in Eq. 5	<i>Halluc</i>	<i>General</i>
High-similarity	<b>5.3</b>	1.2	Temporal	3.5	1.1	Far ( $d_i$ )	<b>5.3</b>	1.2	Visual ( $\mathbf{v}_i^l$ )	3.7	1.3
Low-similarity	0.2	<b>-0.1</b>	Visual	3.9	0.7	Near ( $-d_i$ )	3.8	<b>-0.7</b>	Output ( $\mathbf{p}_i^l$ )	<b>5.3</b>	1.2
Combination	2.4	0.3	Mixed	<b>5.3</b>	<b>1.2</b>	Equal ( $\frac{1}{N}$ )	4.6	0.4			

(a) **Augmentation group.**  $\mathcal{V}$  generated by only high-similarity augmentations ensures all clips are close-semantic with the original clip.  
 (b) **Augmentation diversity.** Diverse high-augmentations enlarge the chance of true-rejected samples related to the questions.  
 (c) **Weight  $\alpha_i$ .** Enhance weight based on the farthest clip ( $\alpha_i$  is proportional to  $d_i$ ) is better for avoiding false-rejected issue.  
 (d)  **$d_i$  computation.** Computing  $d_i$  based on LLM’s output  $\mathbf{p}_i$  is better than only visual  $\mathbf{v}_i$  for the extra question infos.

Table 3. **The ablation study of key components in PaMi-VDPO.** (a)-(b) analyze the candidate set  $\mathcal{V}$  and (c)-(d) analyze the question-aware weight  $\alpha_i$ . *Halluc* and *General* indicates the average performance gap relative to the base model on the hallucinations and general benchmarks. Best results and default settings are reported in **Bold** and **gray**. The performance degradation is highlighted in **red**.

*OV*) is included in both for reference.

**Hallucination benchmarks.** Table 1 presents the hallucination performance comparison of our methods with other training methods, *i.e.* SFT, DPO, and VDPO. Note that we keep the training data to be the same for SFT, DPO, VDPO and our PaMi-VDPO. We can observe two main findings: (i) *preference learning outperforms the standard SFT on both hallucination benchmarks*; (ii) *Our PaMi-VDPO shows better performance than both DPO and native VDPO across different backbones*. More importantly, unlike DPO, our method does not require pre-constructing preference data, reducing usage costs while also avoiding hallucinations introduced by data construction.

**General benchmarks.** Table 2 compares ours with different learning methods on the general benchmarks. Although SFT shows limited gains on the hallucination benchmark, it consistently improves general tasks. In contrast, DPO and VDPO suffer notable drops, especially VDPO, which declines by 2% on Video-MME due to false-rejected samples disrupting alignment. By avoiding this issue, our method achieves stable improvements on general benchmarks.

### 6.3. Ablation Study

In this section, we conduct the extensive experiments to ablate the effect of our proposed modules. We use the LLaVA-OV-7B [13] as our baseline model. As analyzed in Section 5, the effectiveness of PaMi-VDPO relies on the two key components: the constructed rejected candidates set  $\mathcal{V}$  and prompt-dependent weight  $\alpha_i$ . We ablate the two components in Table 3 to prove that the effectiveness of the close-to-far strategy.

#### 6.3.1. Rejected Candidates Set

As analyzed in Section 5, the augmentations used to generate  $\mathcal{V}$  have two key properties: high similarity and diversity, which are ablated in Table 3a and Table 3b, respectively.

**Augmentation Group.** Table 3a compares three augmentation settings for constructing  $\mathcal{V}$  (details in Section 4.2.1): (i) High-similarity: only high-similarity augmentations; (ii) Low-similarity: only low-similarity augmentations; (iii) Combination: a mix of both, with equal proportions. For all settings, we fix  $|\mathcal{V}| = 2$  (further ablations in the **supplementary materials** confirm this suffices for strong performance).

Results show that high-similarity augmentations achieve the best performance, aligning with findings in Section 4.2.2 and Fig. 3 (b). In the combination setting, the farthest clip (typically low-similarity) is more likely to be selected due to prompt-aware weighting. However, our preference learning across the entire candidate set mitigates the noise from low-similarity clips, leading to a significantly higher performance gain than using only low-similarity augmentations (*e.g.*, +2.4% vs. +0.2% on the hallucination benchmark), demonstrating the robustness of our method.

**Augmentation Diversity.** In Table 3b, we evaluate the effect of the augmentation diversity: (i) Temporal: only augment clips in the temporal dimension (Shuffle, Reverse, Rate); (ii) only augment clips in the visual dimension (Crop, D-Clip); (iii) Mixed: some clips are augmented in the temporal dimension while others are in the visual dimension. All augmentations in this study are high-similarity.

Results indicate that the Mixed setting achieves the best performance, as leveraging both temporal and visual augmentations increases the likelihood of generating true-rejected samples that align with different prompt types.

#### 6.3.2. Prompt-aware Weight

The formulation in Eq. 6 shows that the value of question-aware weight  $\alpha_i$  for clip  $\mathbf{v}_i^l$  is related to the distance  $d_i$  of  $\mathbf{v}_i^l$  to the original clip  $\mathbf{v}_w$ , which is ablated in the following.

**Weight  $\alpha_i$  in Eq. 6.** Table 3c compares three different strategies for computing  $\alpha_i$ : (i) Far:  $\alpha_i$  increases as  $d_i$  increases (Eq. 6); (ii) Near:  $\alpha_i$  decreases as  $d_i$  increases (by replacing  $d_i$  with  $-d_i$  in Eq. 6); (iii) Equal:  $\alpha_i = 1/N$ , assigning equal weight to all rejected clips.

The results show that the Far strategy achieves the best trade-off between hallucination mitigation and general tasks. In contrast, the Near strategy performs worse in both cases, as it selects rejected clips that are too similar to the original, making preference learning less effective in distinguishing meaningful differences and degrading alignment.

Although the Equal strategy does not perform as well as Far, it still achieves a notable improvement in hallucination tasks while maintaining general task performance. This suggests that leveraging a diverse set of rejected clips acts as a form of soft regularization, enhancing training stability.

**Distance  $d_i$  in Eq. 5.** In Table 3d, we compare the effect of

method	VideoHallucer			EventHallusion			<b>General</b>
	Basic	Hallu	Overall	Binary	Desc	Avg	
Baseline	<b>84.1</b>	60.8	48.5	61.3	33.2	47.3	67.0
+DPO	<u>82.5</u>	<u>63.2</u>	<u>50.3</u>	<u>66.6</u>	<u>34.8</u>	<u>50.7</u>	<b>67.3</b>
+Ours	82.4	<b>66.5</b>	<b>51.6</b>	<b>67.2</b>	<b>35.9</b>	<b>51.2</b>	<b>67.2</b>

(a) **Dataset.** Generalizability of ours to LLaVA-HOUND-17k [45].

Table 4. **Generalization of our PaMi-VDPO.** *General* represents the average performance across general benchmarks. The best and second-best values are highlighted in **Bold** and Underline, respectively. In addition to the training data and VLLM used in Table 1, *our method is adaptable to various datasets and VLLMs.*

different ways to compute the distance relative to the original clip. Specifically, the Visual way means computing the cosine similarity between the visual features of the original clip  $v_i^w$  and the current rejected clip  $v_i^l$ . For this, we apply the average-pooling to the output frame features for each video clip from the vision encoders of VLLMs. The output way is our default setting defined in Eq. 5, which considers the information from both prompts and the video clips. Results show that the output way outperforms the visual way clearly on the hallucinations benchmarks, *e.g.*, 5.3% vs. 3.7%. For general tasks, both ways achieve stable performance.

#### 6.4. Generalization

We evaluate the generalization of our method on both dataset and backbone aspects in Table 4.

**Dataset.** To assess generalization beyond our training set, we compare our method with DPO on an additional public video preference dataset, LLaVA-HOUND-17k [45], which samples videos from WebVid [1], VIDAL [51], and ActivityNet [2], with preference data generated by GPT-4V.

As shown in Table 4a, both DPO and PaMi-VDPO achieve only marginal improvements on general benchmarks, likely because LLaVA-HOUND-17k overlaps with the SFT data used for LLaVA-OV. However, on both hallucination benchmarks, our method consistently outperforms DPO. Notably, despite LLaVA-HOUND-17k containing 17K preference-labeled samples—more than the 10K SFT samples used in Table 1—the performance gains from training on LLaVA-HOUND-17k are smaller. This highlights a key advantage of PaMi-VDPO: it enables direct preference learning on high-quality SFT data without requiring costly pre-constructed preference labels.

**VLLMs.** Besides LLaVA-OV [13], we further evaluate our method on another VLLM to test its robustness across architectures. Table 4b compares our method with DPO on LongVA-7B [44]. The results show that PaMi-VDPO consistently outperforms DPO across different models and benchmarks, demonstrating its adaptability to varying backbone architectures.

#### 6.5. Qualitative Results

To highlight the advantages of our method over standard DPO, we present a visual comparison in Fig. 7, using two examples from VideoHallucer (**Top**) and EventHallusion(**Bottom**). In the top example, both methods receive

method	VideoHallucer			EventHallusion			<b>General</b>
	Basic	Hallu	Overall	Binary	Desc	Avg	
LongVA-7b [44]	<b>83.9</b>	58.4	46.8	66.5	22.2	44.4	58.7
+DPO	78.5	64.3	48.1	<b>74.6</b>	<u>25.9</u>	<u>50.3</u>	58.9
+Ours	<u>79.6</u>	<b>70.7</b>	<b>50.9</b>	<u>72.9</u>	<b>34.8</b>	<b>53.8</b>	<b>60.8</b>

(b) **VLLM.** Generalizability of PaMi-VDPO on LongVA-7b [44].

Table 4. **Generalization of our PaMi-VDPO.** *General* represents the average performance across general benchmarks. The best and second-best values are highlighted in **Bold** and Underline, respectively. In addition to the training data and VLLM used in Table 1, *our method is adaptable to various datasets and VLLMs.*

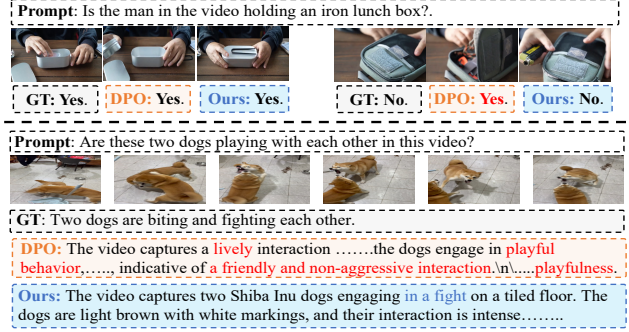


Figure 7. **Qualitative results.** We visualize two samples in VideoHallucer (**Top**) and EventHallusion (**Bottom**). Hallucination responses are highlighted in red. Since our method uses only the video as the variable in preference learning, the generated content is more aligned with the video, thereby reducing hallucinations. More examples can be found in **the supplementary material**.

the same prompt, but the main object in the video changes from a metal box to a fabric box. Our method correctly identifies this change, while DPO fails to adjust its response accordingly. In the bottom example, DPO generates a detailed yet misleading description, assuming that the two dogs are happily playing—an inference likely influenced by LLM biases. *This suggests that standard DPO prioritizes linguistic patterns over actual video understanding.* In contrast, our method directly learns preference signals from video content, allowing it to focus on visual details and produce more accurate responses.

#### 7. Conclusion

In this paper, we introduce Video DPO (VDPO), an online preference learning framework that applies video augmentations to generate rejected video clips, without the need for pre-constructed preference data while improving video-response alignment for reducing hallucinations. We identify the augmentation is the bottleneck in VDPO, and would lead to false-rejected issue, and analyze its impact through extensive empirical studies. To address this, we introduce Prompt-aware Multi-instance VDPO (PaMi-VDPO) to avoid false-rejected issues in a close-to-far way, improving stability and effectiveness. Extensive experiments and ablation studies prove the effect of our method and different modules.

## References

- [1] Max Bain, Arsha Nagrani, G  l Varol, and Andrew Zisserman. Frozen in time: A joint video and image encoder for end-to-end retrieval. In *Proceedings of the IEEE/CVF international conference on computer vision*, pages 1728–1738, 2021. 8
- [2] Fabian Caba Heilbron, Victor Escorcia, Bernard Ghanem, and Juan Carlos Niebles. Activitynet: A large-scale video benchmark for human activity understanding. In *Proceedings of the ieee conference on computer vision and pattern recognition*, pages 961–970, 2015. 8
- [3] Mu Cai, Reuben Tan, Jianrui Zhang, Bocheng Zou, Kai Zhang, Feng Yao, Fangrui Zhu, Jing Gu, Yiwu Zhong, Yuzhang Shang, Yao Dou, Jaden Park, Jianfeng Gao, Yong Jae Lee, and Jianwei Yang. Temporalbench: Towards fine-grained temporal understanding for multimodal video models. *arXiv preprint arXiv:2410.10818*, 2024. 3, 6
- [4] Zhe Chen, Weiyun Wang, Hao Tian, Shenglong Ye, Zhangwei Gao, Erfei Cui, Wenwen Tong, Kongzhi Hu, Jiapeng Luo, Zheng Ma, et al. How far are we to gpt-4v? closing the gap to commercial multimodal models with open-source suites. *Science China Information Sciences*, 67(12):220101, 2024. 6
- [5] Tri Dao, Dan Fu, Stefano Ermon, Atri Rudra, and Christopher R  . Flashattention: Fast and memory-efficient exact attention with io-awareness. *Advances in Neural Information Processing Systems*, 35:16344–16359, 2022. 1
- [6] Xinpeng Ding, Jianhua Han, Hang Xu, Wei Zhang, and Xiaomeng Li. Hilm-d: Towards high-resolution understanding in multimodal large language models for autonomous driving. *arXiv preprint arXiv:2309.05186*, 2023. 1
- [7] Xinpeng Ding, Jianhua Han, Hang Xu, Xiaodan Liang, Wei Zhang, and Xiaomeng Li. Holistic autonomous driving understanding by bird's-eye-view injected multi-modal large models. In *Proceedings of the IEEE/CVF Conference on Computer Vision and Pattern Recognition*, pages 13668–13677, 2024. 1
- [8] Chaoyou Fu, Yuhai Dai, Yongdong Luo, Lei Li, Shuhuai Ren, Renrui Zhang, Zihan Wang, Chenyu Zhou, Yunhang Shen, Mengdan Zhang, et al. Video-mme: The first-ever comprehensive evaluation benchmark of multi-modal llms in video analysis. *arXiv preprint arXiv:2405.21075*, 2024. 6
- [9] Jinlan Fu, Shenzhen Huangfu, Hao Fei, Xiaoyu Shen, Bryan Hooi, Xipeng Qiu, and See-Kiong Ng. Chip: Cross-modal hierarchical direct preference optimization for multimodal llms. *arXiv preprint arXiv:2501.16629*, 2025. 1, 3
- [10] Seongyun Lee, Sue Park, Yongrae Jo, and Minjoon Seo. Volcano: Mitigating multimodal hallucination through self-feedback guided revision. In *Proceedings of the 2024 Conference of the North American Chapter of the Association for Computational Linguistics: Human Language Technologies (Volume 1: Long Papers)*, pages 391–404, 2024. 2
- [11] Sicong Leng, Hang Zhang, Guanzheng Chen, Xin Li, Shijian Lu, Chunyan Miao, and Lidong Bing. Mitigating object hallucinations in large vision-language models through visual contrastive decoding. In *Proceedings of the IEEE/CVF Conference on Computer Vision and Pattern Recognition*, pages 13872–13882, 2024. 1, 2
- [12] Bo Li, Peiyuan Zhang, Kaichen Zhang, Fanyi Pu, Xinrun Du, Yuhao Dong, Haotian Liu, Yuanhan Zhang, Ge Zhang, Chunyuan Li, et al. Lmms-eval: Accelerating the development of large multimodal models, 2024. 6
- [13] Bo Li, Yuanhan Zhang, Dong Guo, Renrui Zhang, Feng Li, Hao Zhang, Kaichen Zhang, Peiyuan Zhang, Yanwei Li, Ziwei Liu, et al. Llava-onevision: Easy visual task transfer. *arXiv preprint arXiv:2408.03326*, 2024. 2, 3, 4, 6, 7, 8, 1
- [14] Chunyuan Li, Cliff Wong, Sheng Zhang, Naoto Usuyama, Haotian Liu, Jianwei Yang, Tristan Naumann, Hoifung Poon, and Jianfeng Gao. Llava-med: Training a large language-and-vision assistant for biomedicine in one day. *arXiv preprint arXiv:2306.00890*, 2023. 1
- [15] Junnan Li, Dongxu Li, Silvio Savarese, and Steven Hoi. Blip-2: Bootstrapping language-image pre-training with frozen image encoders and large language models. *arXiv preprint arXiv:2301.12597*, 2023. 1
- [16] KunChang Li, Yinan He, Yi Wang, Yizhuo Li, Wenhui Wang, Ping Luo, Yali Wang, Limin Wang, and Yu Qiao. Videochat: Chat-centric video understanding. *arXiv preprint arXiv:2305.06355*, 2023. 1
- [17] Kunchang Li, Yali Wang, Yinan He, Yizhuo Li, Yi Wang, Yi Liu, Zun Wang, Jilan Xu, Guo Chen, Ping Luo, et al. Mvbench: A comprehensive multi-modal video understanding benchmark. In *Proceedings of the IEEE/CVF Conference on Computer Vision and Pattern Recognition*, pages 22195–22206, 2024. 6
- [18] Lei Li, Zhihui Xie, Mukai Li, Shunian Chen, Peiyi Wang, Liang Chen, Yazheng Yang, Benyou Wang, and Lingpeng Kong. Silkie: Preference distillation for large visual language models. *arXiv preprint arXiv:2312.10665*, 2023. 1, 2, 3
- [19] Yanwei Li, Chengyao Wang, and Jiaya Jia. Llama-vid: An image is worth 2 tokens in large language models. In *European Conference on Computer Vision*, pages 323–340. Springer, 2024. 6
- [20] Bin Lin, Bin Zhu, Yang Ye, Munan Ning, Peng Jin, and Li Yuan. Video-llava: Learning united visual representation by alignment before projection. *arXiv preprint arXiv:2311.10122*, 2023. 1, 6
- [21] Ji Lin, Hongxu Yin, Wei Ping, Pavlo Molchanov, Mohammad Shoeybi, and Song Han. Vila: On pre-training for visual language models. In *Proceedings of the IEEE/CVF conference on computer vision and pattern recognition*, pages 26689–26699, 2024. 6
- [22] Fuxiao Liu, Kevin Lin, Linjie Li, Jianfeng Wang, Yaser Yacoob, and Lijuan Wang. Mitigating hallucination in large multi-modal models via robust instruction tuning. In *The Twelfth International Conference on Learning Representations*, 2023. 2
- [23] Haotian Liu, Chunyuan Li, Qingyang Wu, and Yong Jae Lee. Visual instruction tuning. *arXiv preprint arXiv:2304.08485*, 2023. 1, 3
- [24] Haotian Liu, Chunyuan Li, Yuheng Li, and Yong Jae Lee. Improved baselines with visual instruction tuning. In *Proceedings of the IEEE/CVF Conference on Computer Vision and Pattern Recognition*, pages 26296–26306, 2024. 1
- [25] Hanchao Liu, Wenyuan Xue, Yifei Chen, Dapeng Chen, Xiutian Zhao, Ke Wang, Liping Hou, Rongjun Li, and Wei Peng.

A survey on hallucination in large vision-language models. *arXiv preprint arXiv:2402.00253*, 2024. 1, 2

[26] Yuanxin Liu, Shicheng Li, Yi Liu, Yuxiang Wang, Shuhuai Ren, Lei Li, Sishuo Chen, Xu Sun, and Lu Hou. Tempcom-pass: Do video llms really understand videos? *arXiv preprint arXiv:2403.00476*, 2024. 4, 6

[27] Fan Ma, Xiaojie Jin, Heng Wang, Yuchen Xian, Jiashi Feng, and Yi Yang. Vista-llama: Reducing hallucination in video language models via equal distance to visual tokens. In *Proceedings of the IEEE/CVF Conference on Computer Vision and Pattern Recognition*, pages 13151–13160, 2024. 1, 2

[28] Muhammad Maaz, Hanoona Rasheed, Salman Khan, and Fahad Shahbaz Khan. Video-chatgpt: Towards detailed video understanding via large vision and language models. *arXiv preprint arXiv:2306.05424*, 2023. 1, 6

[29] Yu Meng, Mengzhou Xia, and Danqi Chen. Simpo: Simple preference optimization with a reference-free reward. *arXiv preprint arXiv:2405.14734*, 2024. 3

[30] OpenAI. Hello gpt-4o. <https://openai.com/index/hello-gpt-4o/>. 2024. 3, 4, 6, 2

[31] Yassine Ouali, Adrian Bulat, Brais Martinez, and Georgios Tzimiropoulos. Clip-dpo: Vision-language models as a source of preference for fixing hallucinations in l1lms. In *European Conference on Computer Vision*, pages 395–413. Springer, 2024. 3

[32] Renjie Pi, Tianyang Han, Wei Xiong, Jipeng Zhang, Runtao Liu, Rui Pan, and Tong Zhang. Strengthening multimodal large language model with bootstrapped preference optimization. In *European Conference on Computer Vision*, pages 382–398. Springer, 2024. 3

[33] Rafael Rafailov, Archit Sharma, Eric Mitchell, Christopher D Manning, Stefano Ermon, and Chelsea Finn. Direct preference optimization: Your language model is secretly a reward model. *Advances in Neural Information Processing Systems*, 36, 2024. 2, 3

[34] John Schulman, Filip Wolski, Prafulla Dhariwal, Alec Radford, and Oleg Klimov. Proximal policy optimization algorithms. *arXiv preprint arXiv:1707.06347*, 2017. 3

[35] Gemini Team, Petko Georgiev, Ving Ian Lei, Ryan Burnell, Libin Bai, Anmol Gulati, Garrett Tanzer, Damien Vincent, Zhufeng Pan, Shibo Wang, et al. Gemini 1.5: Unlocking multimodal understanding across millions of tokens of context. *arXiv preprint arXiv:2403.05530*, 2024. 6

[36] Fei Wang, Wenzuan Zhou, James Y Huang, Nan Xu, Sheng Zhang, Hoifung Poon, and Muhan Chen. mdpo: Conditional preference optimization for multimodal large language models. 2024. 1, 2, 3

[37] Yuxuan Wang, Yueqian Wang, Dongyan Zhao, Cihang Xie, and Zilong Zheng. Videohallucer: Evaluating intrinsic and extrinsic hallucinations in large video-language models. *arXiv preprint arXiv:2406.16338*, 2024. 4, 6, 1

[38] Junbin Xiao, Xindi Shang, Angela Yao, and Tat-Seng Chua. Next-qa: Next phase of question-answering to explaining temporal actions. In *Proceedings of the IEEE/CVF Conference on Computer Vision and Pattern Recognition (CVPR)*, pages 9777–9786, 2021. 4, 6

[39] Yuxi Xie, Guanzhen Li, Xiao Xu, and Min-Yen Kan. V-dpo: Mitigating hallucination in large vision language models via vision-guided direct preference optimization. In *Findings of the Association for Computational Linguistics: EMNLP 2024*, pages 13258–13273, 2024. 1, 3

[40] Shukang Yin, Chaoyou Fu, Sirui Zhao, Tong Xu, Hao Wang, Dianbo Sui, Yunhang Shen, Ke Li, Xing Sun, and Enhong Chen. Woodpecker: Hallucination correction for multimodal large language models. *Science China Information Sciences*, 67(12):220105, 2024. 2

[41] Qifan Yu, Juncheng Li, Longhui Wei, Liang Pang, Wentao Ye, Bosheng Qin, Siliang Tang, Qi Tian, and Yueting Zhuang. Hallucidoctor: Mitigating hallucinatory toxicity in visual instruction data. In *Proceedings of the IEEE/CVF Conference on Computer Vision and Pattern Recognition*, pages 12944–12953, 2024. 2

[42] Tianyu Yu, Haoye Zhang, Yuan Yao, Yunkai Dang, Da Chen, Xiaoman Lu, Ganqu Cui, Taiwen He, Zhiyuan Liu, Tat-Seng Chua, and Maosong Sun. Rlaif-v: Aligning mllms through open-source ai feedback for super gpt-4v trustworthiness. *arXiv preprint arXiv:2405.17220*, 2024. 1, 2, 3

[43] Jiacheng Zhang, Yang Jiao, Shaoxiang Chen, Jingjing Chen, and Yu-Gang Jiang. Eventhallusion: Diagnosing event hallucinations in video llms. *arXiv preprint arXiv:2409.16597*, 2024. 6, 1, 2

[44] Peiyuan Zhang, Kaichen Zhang, Bo Li, Guangtao Zeng, Jingkang Yang, Yuanhan Zhang, Ziyue Wang, Haoran Tan, Chunyuan Li, and Ziwei Liu. Long context transfer from language to vision. *arXiv preprint arXiv:2406.16852*, 2024. 6, 8

[45] Ruohong Zhang, Liangke Gui, Zhiqing Sun, Yihao Feng, Keyang Xu, Yuanhan Zhang, Di Fu, Chunyuan Li, Alexander Hauptmann, Yonatan Bisk, et al. Direct preference optimization of video large multimodal models from language model reward. *arXiv preprint arXiv:2404.01258*, 2024. 1, 2, 3, 8

[46] Yuanhan Zhang, Bo Li, haotian Liu, Yong jae Lee, Liangke Gui, Di Fu, Jiashi Feng, Ziwei Liu, and Chunyuan Li. Llava-next: A strong zero-shot video understanding model, 2024. 1

[47] Yuanhan Zhang, Jinming Wu, Wei Li, Bo Li, Zejun Ma, Ziwei Liu, and Chunyuan Li. Video instruction tuning with synthetic data, 2024. 3, 6

[48] Linxi Zhao, Yihe Deng, Weitong Zhang, and Quanquan Gu. Mitigating object hallucination in large vision-language models via classifier-free guidance. *arXiv preprint arXiv:2402.08680*, 2024. 1, 2

[49] Yiyang Zhou, Chenhang Cui, Jaehong Yoon, Linjun Zhang, Zhun Deng, Chelsea Finn, Mohit Bansal, and Huaxiu Yao. Analyzing and mitigating object hallucination in large vision-language models. In *NeurIPS 2023 Workshop on Instruction Tuning and Instruction Following*. 1, 2

[50] Zhi-Hua Zhou. Multi-instance learning: A survey. *Department of Computer Science & Technology, Nanjing University, Tech. Rep*, 2, 2004. 5

[51] Bin Zhu, Bin Lin, Munan Ning, Yang Yan, Jiaxi Cui, HongFa Wang, Yatian Pang, Wenhao Jiang, Junwu Zhang, Zongwei Li, et al. Languagebind: Extending video-language pretraining to n-modality by language-based semantic alignment. *arXiv preprint arXiv:2310.01852*, 2023. 8

- [52] Deyao Zhu, Jun Chen, Xiaoqian Shen, Xiang Li, and Mohamed Elhoseiny. Minigpt-4: Enhancing vision-language understanding with advanced large language models. *arXiv preprint arXiv:2304.10592*, 2023. [1](#)
- [53] Ke Zhu, Liang Zhao, Zheng Ge, and Xiangyu Zhang. Self-supervised visual preference alignment. In *Proceedings of the 32nd ACM International Conference on Multimedia*, pages 291–300, 2024. [3](#)

# PaMi-VDPO: Mitigating Video Hallucinations by Prompt-Aware Multi-Instance Video Preference Learning

## Supplementary Material

Numbers	VideoHallucer	EventHallusion	General	AVG
1	51.1	50.0	65.9	55.7
2	53.8	53.2	68.2	58.4
3	53.9	53.5	68.0	58.5
4	54.1	53.2	68.4	58.5
Baseline	48.5	47.3	67.0	54.3

Table I. **Ablation Study of numbers of candidate clips in the set  $\mathcal{V}$ .** We use the high-similarity and Mixed setting for set construction. We find that setting the number to 2 can achieve good performance.

Numbers	VideoHallucer	EventHallusion	General	AVG
(1),(4)	52.6	52.5	68.5	57.9
(1),(5)	52.8	51.7	68.7	57.7
(1),(6)	53.8	53.0	67.9	58.2
(3),(4)	53.8	53.2	68.2	58.4
(3),(5)	53.2	52.1	68.3	57.9
(3),(6)	53.6	53.4	67.2	58.1
Baseline	48.5	47.3	67.0	54.3

Table II. **Ablation Study of different combinations of augmentations.** We use the high-similarity and Mixed setting for set construction. With the combination of (3) and (4) for the set construction, we can achieve the best performance.

## A. More Ablation Study

**The number of clips in the Set.** Table I presents the ablation study of number of candidate clips in the set, *i.e.*,  $|\mathcal{V}|$ . The results indicate that as the number of augmented clips in the set increases, the model’s average performance steadily improves. Notably, the performance gain is most significant when increasing the number from 1 to 2, rising from 55.7 to 58.4. This highlights the advantage of our approach in constructing multiple clips, as having only one clip reduces the method to standard VDPO.

It is also worth noting that while increasing the number from 2 to 4 results in further improvements, the gains are less pronounced. This suggests that with a carefully designed augmentation strategy ensuring sufficient diversity, a small number of clips can effectively fulfill our method’s objectives. Considering the additional training cost associated with increasing the number of clips, we adopt number = 2 as our default setting.

**Effect of different combinations of augmentations.** As illustrated in Section. 4 of our manuscript, We apply the following video augmentations to construct rejected clips:

**(1) Crop** – randomly cropping less than 20% of the frame from the original video; **(2) D-video** – randomly selecting



Figure I. **Qualitative results on VideoHallucer** [37]. We visualize two examples for semantic (**Top**) and temporal (**Bottom**) hallucinations respectively. Hallucination responses are highlighted in red. Since our method uses only the video as the variable in preference learning, the generated content is more aligned with the video, thereby reducing hallucinations.

clips from another video from the training data; **(3) D-Clip** – selecting another clip from the same long video with the original video clip. **(4) Shuffle** – shuffling the temporal order of the original video clip; **(5) Reverse** – reversing the original temporal order; **(6) Rate** – sampling frames from the original video clip at a different frame rate; **(7) Combination** – applying two ways sampled from previous augmentation strategies. From the previous analysis, we should choose one augmentation from (1) and (3) and one augmentation from (4), (5) and (6) for good performance. Here, we conduct a detailed ablation study of which combination can achieve the best performance. As shown in Table II, the combination of (3) and (4) can achieve the best performance. Note that even the worst combination can also outperform the baseline model LLaVA-OV-7B [13] over 3.4%, which proves the effectiveness of our method.

## B. More Visualization Results

In this section, we provide more visualization comparison with DPO on both VideoHallucer [37] and EventHallusion [43].

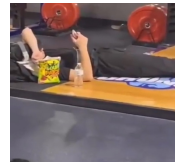
**VideoHallucer.** Fig. I illustrates two types of hallucinations: visual semantic (Top) and temporal (Bottom). In the visual semantic case, the model must generate responses based on two different videos given the same prompt. In the temporal case, the model generates responses based on two different prompts for the same video.

The results demonstrate that PaMi-VDPO accurately generates responses in both scenarios, effectively grounding

**Prompt:** Is the man doing exercises in this video?



**GT:** No. A man is sleeping on the floor in the gym.



**Ours:** The video takes place in a gym setting, featuring a person lying on their back on a weightlifting platform. The individual is dressed in black athletic attire and appears to be resting or possibly recovering from a workout. Surrounding the person are various items including a black bag, an orange water bottle, and a yellow snack packet. In the background, there are multiple weightlifting racks with weights of different sizes, predominantly red and yellow, indicating a well-equipped gym environment. The person remains mostly stationary throughout the video, with minimal movement, suggesting they are either resting or taking a break. The gym floor is gray, and the weightlifting platform has a yellow and blue surface. The lighting in the gym is bright, and the overall atmosphere suggests a typical fitness routine. No significant changes occur in the scene, and the focus remains on the individual and their immediate surroundings. The video captures a moment of rest within a fitness context, highlighting the importance of recovery and hydration during exercise routines.

**GPT4-o Judgement:** Yes. The model's output describes an individual lying on a weightlifting platform in a gym setting, appearing to be resting or recovering from a workout. This is consistent with the ground-truth event of a man sleeping on the floor in the gym, as both describe a scene of a person lying down and at rest in a gym environment. The action of being at rest aligns with the idea of sleeping.

**DPO:** The video takes place in a gym setting, featuring a weightlifting platform with various weight plates and barbells arranged around it. They are positioned horizontally across the platform, with their legs bent at the knees and feet flat against the ground. In front of the individual, there is a colorful towel spread out on the platform, which serves as a makeshift mat. To the left side of the individual, there is a collection of items: a large beige backpack, a black bag with red accents, and a bright orange water bottle. These items are neatly arranged, suggesting that the person has prepared for their workout session. As the video progresses, the individual begins to engage in a stretching routine. They lift one leg at a time, extending it upwards while maintaining a straight posture, indicating a focus on flexibility and muscle preparation. This sequence repeats several times, alternating between legs, emphasizing the importance of thorough warm-up exercises before engaging in more strenuous activities. Throughout the video, the overall atmosphere suggests a dedicated approach to fitness, highlighting the importance of proper preparation and flexibility exercises in weightlifting and general exercise routines.

**GPT4-o Judgement:** No. The model's output describes an individual engaging in a stretching routine, focusing on flexibility exercises. In contrast, the ground-truth event states that a man is sleeping on the floor in the gym. These two events are not consistent, as one involves physical activity, and the other involves inactivity (sleeping).

Figure II. Qualitative results on EventHallusion [43]. We compare the visualization results of DPO and our PaMi-VDPO. Hallucination responses are highlighted in red. GPT4-o Judgement indicates that using GPT-4o [30] to assess whether the response is aligned with the video clip.

its predictions in the visual content. In contrast, DPO exhibits hallucinations, such as incorrect color recognition and misinterpretation of temporal sequences.

**EventHallusion.** Fig. II showcases an event-level hallucination, where a man is lying on the floor in a gym. Due to inherent biases in the pretrained LLM—*i.e.*, associating gyms primarily with exercise—the DPO-trained model generates hallucinated descriptions misaligned with the actual scene.

In contrast, PaMi-VDPO is explicitly trained to ground preference judgments in video content, enabling it to produce responses that accurately reflect the observed events.

## C. Preference Data Construction

To construct the preference data for DPO, we conduct a series of augmentations (see in Section A) to the original clip to obtain the augmented clips. Then, we input the augmented clip and original prompt to the baseline model, *i.e.*, LLava-OV-7B [13], to generate the candidate rejected responses. After that, we use the prompt defined in Fig. III to leverage GPT-4o [30] to give the matching score for each candidate rejected response. Finally, we choose the response whose score is larger than 4.0 as the chosen and those whose score is smaller than 3.0 as the rejected.

Prompting GPT4-o to judge the preference score for predictions

```
messages = [{"role": "system", "content": "You are an intelligent chatbot designed for evaluating the correctness of generative outputs for question-answer pairs. Your task is to compare the predicted answer with the correct answer and determine if they match meaningfully. Here's how you can accomplish the task: \n\nGiven the following inputs: 1. **Question**: {question} 2. **Ground Truth Answer**: {answer} 3. **Model Predicted Answer**: {prediction} Your task is to evaluate the model's predicted answer against the ground truth answer, based on the question. Consider the following criteria for evaluation: - **Relevance**: Does the predicted answer directly address the question posed? - **Accuracy**: Compare the predicted answer to the ground truth answer. Does the prediction accurately reflect the information given in the ground truth answer without introducing factual inaccuracies? - **Clarity**: Assess the clarity of the predicted answer. Look for issues such as repetition, unclear descriptions, or any grammatical errors that could hinder understanding. - **Completeness**: Determine if the predicted answer fully covers the scope of the ground truth answer. Does it leave out critical information or does it include all necessary details? **Output Format**: Explanation: <brief judgement of prediction> Score: <a integer score of quality from 1-5> \n\nFor example, your response should look like this: {'pred': 'yes', 'score': 2.8}."},]
```

Figure III. Prompts we use to prompt GPT- 4o to generate the preference score between the predictions and the ground-truths.